AIAA 2000-3978
A Study of Airline Passenger Susceptibility to Atmospheric Turbulence Hazard

Eric C. Stewart
NASA Langley Research Center
Hampton, VA

Atmospheric Flight Mechanics Conference
14-17 August 2000
Denver, CO

A STUDY OF AIRLINE PASSENGER SUSCEPTIBILITY TO ATMOSPHERIC TURBULENCE HAZARDS

Eric C. Stewart*

NASA Langley Research Center
Hampton, VA 23681-2199

Abstract

A simple, generic, simulation math model of a commercial airliner has been developed to study the susceptibility of unrestrained passengers to large, discrete gust encounters. The math model simulates the longitudinal motion to vertical gusts and includes (1) motion of an unrestrained passenger in the rear cabin, (2) fuselage flexibility, (3) the lag in the downwash from the wing to the tail, and (4)unsteady lift effects. Airplane and passenger response contours are calculated for a matrix of gust amplitudes and gust lengths of a simulated mountain rotor. A comparison of the model -predicted responses to data from three accidents indicates that the accelerations in actual accidents are sometimes much larger than the simulated gust encounters.

Nomenclature

alt	altitude, ft
a_z	acceleration of cg vertically downward, g's
a_{aft}	acceleration at aft passenger cabin, g's
$C_{D,i}$	total drag coefficient of ith surface, non-dimensional
$C_{L,i}$	lift coefficient of ith surface, non-dimensional
$C_{L,\alpha}$	lift curve slope of airplane, per radian
$C_{L\alpha,t}$	lift curve slope of tail, per radian
$C_{Do,t}$	zero lift drag coefficient of the tail, non-dimensional
c_w	mean aerodynamic chord of wing, ft
d_{fall}	equivalent fall height in a 1-g gravity field (see eqn. 28) , ft
f	frequency of flexible fuselage mode, Hz
F_s	force due to flexible fuselage spring, lb
$F_{x,i}$	component of force along X body axis (i=w, t, T), lb
$F_{z,i}$	component of force along Z body axis (i=w, t, ta, T), lb
g	acceleration of gravity, 32.2 ft/sec^2
h	position of unrestrained mass above aft cabin floor, ft
$\dot{h}_c$	collision velocity with the floor or ceiling, fps
I_y	moment of inertia about y (pitch) axis, slug-ft^2
k	flexible fuselage spring constant, lb/ft
k_t	efficiency factor of the tail, non-dimensional
k_q	pitch rate gain in autopilot, radians/(radians/sec)
k_θ	pitch angle gain in autopilot, radians/radian
k_h	altitude hold feedback gain, radians/ft
$k_{\delta e}$	elevator effectiveness, non-dimensional
l_g	gust length (see equation 29), ft
m	mass of wing-body, slugs
m_e	equivalent mass of aeroelastic structure, slugs
Δn_{cg}	delta normal acceleration of center of gravity, g's
Δn_{aft}	delta normal acceleration of aft passenger cabin, g's
q	pitch rate, radians/second
$\bar{q}$	dynamic pressure, psf
r	radial distance from center of mountain rotor (see equation 29), ft
R	ratio of x position of aft passenger cabin to tail length, non-dimensional

*Aerospace Engineer, Senior Member AIAA

S_w	wing area, 1994 ft^2
t	time, seconds
Δt	lag in wing downwash reaching the tail, seconds
T_{θ_2}	plunge motion time constant ($m/\rho V S_w C_{L_\alpha}$), seconds
u_o	component of inertial velocity along X body axis, fps
V	true airspeed, fps
V_{max}	maximum tangential velocity of wind rotor (see equation 28), fps
V_{tan}	tangential velocity of wind rotor (see equation 28), fps
W	weight of airplane, lb
w_o	component of inertial velocity along Z body axis, fps
x_i	x location of point of application of the ith force component, ft
y_{trim}	vertical displacement of horizontal tail due to aeroelastic effects at trim flight condition, ft
Δy	change in length of spring from trim length, ft
z_i	z location of point of application of ith force component, ft
α	angle of attack, radians or degrees
$\frac{\partial \varepsilon}{\partial \alpha}$	downwash parameter, non-dimensional
δ_e	elevator deflection, radians
δ_{cc}	component of elevator deflection due to simulated autopilot, radians
θ	pitch angle, radians or degrees
ρ	density of air, $slug/ft^3$
$\Delta\gamma$	change in flight path angle, radians
ε	inclination of thrust axis with respect to x body axis (positive up), radians
ω_n	natural frequency of aeroelastic mode, radians/sec

Subscripts:

w	wing
t	(horizontal) tail
ta	(horizontal) tail aerodynamic
T	thrust
g	gust
e	earth (axis system)
b	body (axis system)
i	ith aerodynamic component
ic	initial value
aft	in the aft passenger cabin

Operators

Δ	change
.	first derivative with respect to time
..	second derivative with respect to time
$f_L()$	non-linear lift function
$f_D()$	non-linear drag function

Introduction

The NASA has initiated an aviation safety program aimed at reducing the accident rate of transport airplanes. One element of this program is concerned with the fatalities and injuries caused by encounters with turbulence. Although the literature is full of studies on airplane gust loads, these studies have primarily been concerned with the structural integrity of the airplanes and certification issues. However, in most accident scenarios the airplane structure is not damaged, but flight attendants and unrestrained passenger are injured or killed[1]. Often the airplane unexpectedly encounters a discrete gust of only a few seconds duration while flying in otherwise relatively calm air. A study that specifically addresses the interaction of the gust/airplane/autopilot/pilot is needed help identify critical factors in a typical accident. For example, the parameter(s) that best describe the gust characteristic(s) that induce accidents need to be identified. Once these parameters are identified, sensors such a radar and lidair can be designed to detect and avoid dangerous gusts. In addition, the responses of the airplane, autopilot, and pilot that contribute to the problem need to be identified. Once these responses are identified, improvements to the autopilot and piloting procedures may be possible.

A three step procedure was used to study these factors. First, a simulation math model was developed to explore the response of unrestrained passengers to gusts of various shapes and sizes. This model was generic with a minimum of airplane characteristics. However, the model included representations of such things as non-linear aerodynamics, an autopilot, fuselage bending, the lag in the downwash from the wing to the tail, unsteady lift effects on the wing, and inelastic collisions of unrestrained objects with the interior of the rear cabin.

The second step was to analyze the flight data recorder (FDR) measurements from three recent turbulence accidents involving domestic commercial

airliners. Approximate gust profiles were produced from estimated airplane aerodynamic and mass characteristics plus the measured parameters on the flight data recorders such as vertical acceleration and pitch attitude.

The third and final step was to compare the accident gust profiles and airplane responses to those predicted by the math model.

This paper presents a short description of the simulation math model and various gust wave shapes that were investigated. The simulation response calculations were then summarized into constant response contours as a function of gust length and amplitude. Next, the equations used to analyze the FDR data are presented along with the extracted gust velocities. Finally, the simulation calculations and the FDR data are compared, and some observations are made.

Simulation Studies

Math Model:

The equations of motion are written in a body axis system that is free to translate and pitch in a vertical plane. The airplane is modeled as a wing-body mass connected by a spring to the effective horizontal tail mass. The airplane mass is acted on by the wing body aerodynamic forces, gravity forces, the thrust forces, the X aerodynamic force of the horizontal tail, and a Z tail force produced by the connecting spring. The effective tail mass is acted on by the Z aerodynamic tail force, the connecting spring force, and gravity. A diagram of model is presented in figure 1. The equations of motion for this system are given below:

Airplane wing-body:

$$\sum_i F_{x,i} - mg\sin(\theta) = m(\dot{u}_o + qw_o) \quad (1)$$

$$\sum_i F_{z,i} + mg\cos(\theta) = m(\dot{w}_o - qu_o) \quad (2)$$

$$\sum_i F_{x,i} z_i - \sum_i F_{z,i} x_i = I_y \dot{q} \quad (3)$$

where i = w,t,T

Flexible tail:

$$\Delta\ddot{y} = \frac{F_s}{m_e} + \frac{F_{z,ta}}{m_e} - ga_z - g + x_t\dot{q} \quad (4)$$

The X aerodynamic forces for the wing and tail in equations (1) and (3) are derived from the lift and drag

$$F_{x,i} = \bar{q}S_w[-C_{D,i}\cos(\alpha_i) + C_{L,i}\sin(\alpha_i)] \quad (5)$$

where i=w,t

with the non-linear, table-lookup aerodynamic characteristics of the wing:

$$C_{L,w} = f_L(\alpha_w) \text{ and } C_{D,w} = f_D(\alpha_w) \quad (6)$$

and the estimated aerodynamic characteristics of the tail

$$C_{L,t} = C_{L\alpha,t}\alpha_t \text{ and } C_{D,t} = C_{Do,t} + k_t C_{L,t}^2 \quad (7)$$

The force components for the thrust are simply:

$$F_{x,T} = Thrust * \cos(\varepsilon) \quad (8)$$

$$F_{z,T} = -Thrust * \sin(\varepsilon) \quad (9)$$

The aerodynamic Z forces for the wing and the elastic tail are:

$$F_{z,i} = \bar{q}S_w[-C_{L,i}\cos(\alpha_i) - C_{D,i}\sin(\alpha_i)] \quad (10)$$

where i=w,ta

The Z force from the tail ($F_{Z,t}$) that is transmitted to the wing-body through the simulated spring is not the same as the aerodynamic tail force ($F_{z,ta}$) given in equation (10). It is, instead equal and opposite F_S in equation (4) above:

$$F_{Z,t} = -F_s = -k(y_{trim} + \Delta y) \quad (11)$$

The spring constant, k, in equation (10) and the effective tail mass, m_e, in equation (4) were estimated as follows. First, a natural frequency of the elastic tail system was assumed, i.e. f = 3 Hz. Then a structural stiffness was calculated by assuming that the tail would deflect a given ratio, R=.02, of the tail length if loaded with the entire weight of the airplane. That is,

$$k = (mg)/(-x_t * R) \quad (12)$$

Finally, the effective mass is calculated from the spring constant and the assumed natural frequency

$$m_e = \frac{k}{(2\pi f)^2} \quad (13)$$

The angles of attack on the wing and tail are, of course, critical to the proper calculations of the aerodynamic forces and moments. The angle of attack at the wing was calculated from the following equation:

$$\alpha_w = \tan^{-1}\left(\frac{w_w}{u_w}\right) \quad (14)$$

where the velocity components for the wing are a straightforward sum of the inertial components and the gust components:

$$u_w = u_o + u_g \quad (15)$$

$$w_w = w_o + w_g \quad (16)$$

The primed parameters are the unsteady lift effects represented by the approximate formulas[2]:

$$w_o' = w_o(1-.36e^{-\frac{t}{\tau_o}}) \text{ and } w_g' = w_g(1-e^{-\frac{t}{\tau_g}}) \quad (17)$$

with

$$\tau_o = \frac{3c_w}{2V} \quad \text{and} \quad \tau_g = \frac{3c_w}{4V} \quad (18)$$

The velocity components for tail are more complicated even though unsteady lift effects are ignored. For example, the gust hits the tail slightly after it hits the wing. Also, the velocity at the tail is modified by the downwash from the wing. Of course, the pitching motion of the airplane induces a vertical velocity at the tail that is primarily responsible for the pitch damping[3]. Adding the flexible tail degree of freedom adds more terms to these basic effects. The vertical motion of elastic tail induces a vertical velocity component at the tail that is responsible for damping of this structural mode. In addition, the deflection of the flexible tail surface changes the incidence angle of the tail and reduces the effective angle of attack of the tail. All these effects are modeled in the following equations for the velocity components and angle of attack at the tail:

$$u_t = u_o + u_g(t-\Delta t) + z_t * q \quad (19)$$

$$w_t = w_o - \frac{\partial \varepsilon}{\partial \alpha} w_o(t-\Delta t) \ldots$$

$$+ (1-\frac{\partial \varepsilon}{\partial \alpha}) w_g(t-\Delta t) - x_t q + \Delta \ddot{y} \quad (20)$$

where the $(t-\Delta t)$ notation indicates the parameter is evaluated at an earlier time [with $\Delta t = (x_w - x_t)/V$] to account for the time difference in effects at the tail and the wing. All the other parameters are evaluated at the current time t.

The angle of attack at the tail was calculated from the above velocity components plus two additional terms:

$$\alpha_t = a\tan^{-1}(\frac{w_t}{u_t}) + k_{\delta e}\delta e + \frac{2(\Delta y + y_{trim})}{-x_t} \quad (21)$$

The second term on the right hand side of equation (21) is the effect of the elevator (used from trimming the simulated airplane and as the autopilot effector) , while the third term is the effect of the flexible tail degree of freedom assuming a quadratic structural deflection curve.

The autopilot control law contained feedback terms for the pitch rate, pitch attitude, and altitude:

$$\delta_{ec} = k_q q + k_\theta(\theta - \theta_{trim}) + k_h(alt - alt_{trim}) \quad (22)$$

The commanded elevator was passed through a 14 radians/sec first-order actuator model and added to the trimmed elevator position.

$$\delta_e = \delta_{ec} + \delta_{e,trim} \quad (23)$$

In order to simulate the collisions of an unrestrained passenger with the ceiling and floor, an auxiliary calculation was made. The first step was to calculate the normal acceleration at an estimated extreme aft cabin position:

$$a_{aft} = -a_z + 0.8x_t\dot{q} - (0.8)^2\Delta\ddot{y} \quad (24)$$

were the 0.8 factor was the estimated ratio of the aft cabin location to the tail location, x_t .The factor is squared because the deflection curve of the rear fuselage was assumed to be quadratic. Whenever the unrestrained body (passenger) was not in contact with either the floor or the ceiling ($0 < h < 4$), its acceleration relative to the (accelerating) cabin floor or ceiling was

$$\ddot{h} = -a_{aft} \quad (25)$$

This acceleration was then integrated to produce the relative velocity and position. The inelastic collisions with the floor and ceiling were simulated by setting $\dot{h} = 0$ whenever

$$h \le 0 \text{ and } (\dot{h} < 0 \text{ or } \ddot{h} < 0) \quad (26)$$

$$\text{or } h \ge 4 \text{ and } (\dot{h} > 0 \text{ or } \ddot{h} > 0) \quad (27)$$

This simulated a purely inelastic collision (no rebound) of the passenger with the interior of the cabin. The 4 (ft) constant in equation (27) was a compromise between the distance between a passenger's head while standing in the aisle and the ceiling and the much longer distance from the ceiling to the floor. The collision velocity with the floor or ceiling, $\dot{h}_c$, was transformed into an equivalent height of a fall in a normal 1-g gravity field using

$$d_{fall} = \frac{(\dot{h}_c + 4a_{aft})^2}{2g} \quad (28)$$

where the $4a_{aft}$ term is added to account for the fact that the floor (or ceiling) is either accelerating away from or toward the passenger when he impacts the floor (or ceiling). The constant of 4 is based on the assumption that the body of the passenger deforms 3 inches upon impact.

Gust inputs:

Several different gust shapes were investigated including "1-cosine," simple ramps, sawtooth, sine waves, and a mountain rotor, figure 2. However, only results from the mountain rotor are presented herein. These results are fairly typical of the other wave shapes if they are compared on the basis of

a consistent set of gust lengths and amplitudes. The mountain rotor was represented by a simple algebraic relationship that was a function of two parameters: gust amplitude, V_{max}, and gust length, l_g. The general equation was

$$V_{tan} = V_{max} \frac{6\left(\frac{r}{l_g}\right)}{\left[5+\left(\frac{r}{l_g}\right)^6\right]} \qquad (29)$$

where r is the radial distance of the airplane from the center of rotation of the rotor. The tangential velocity, V_{tan}, was transformed in to a vertical and horizontal velocity before being applied to the airplane math model. However, since the airplane was initially set to go through the center of the rotor and because the simulated airplane did not translate vertically any significant distance, the gust velocity was almost entirely vertical as will be seen later. A sketch of the vertical velocity is presented in figure 3 for the assumed condition of no vertical translation of the airplane.

Simulated Responses:

The above equations were translated into a Matlab V4.2 Simulink block diagram for solution. The model was trimmed to a cruise flight condition (Mach =0.8 at 30,000 ft) by an iterative routine that determined the trim thrust, angle of attack, elevator position, and spring deflection to produce zero accelerations in level flight. The simulated airplane characteristics are presented in table I.

A time history of a typical gust penetration is shown in figure 4. All the gust responses shown are for gusts that have a negative peak followed by a positive peak. As can seen in the figure, the gust input, Δw_g, has peaks of almost exactly +/-100 fps indicating that there was very little vertical translation away from the center of the rotor by the fast moving airplane. The maximum change in angle of attack was about 7 degrees which did not stall the wing since its initial trim angle of attach was less than 1 degree. The normal acceleration at the c.g, Δn_{cg}, and the acceleration at the aft passenger location, Δn_{aft}, are practically equal because the illustrated gust length of 500 ft is so long that the pitching motion, $\Delta\theta$, is relatively slow. This was not true for shorter gust lengths.

The change in true airspeed, ΔV, was much less than the maximum gust velocity of 100 fps because the latter was nearly perpendicular to the true airspeed of approximately 800 fps. The structural deflection of the horizontal tail, Δy, was relatively small (less than 0.2 feet) indicating that the simulated airplane was relatively stiff. Since the change in the acceleration in the aft cabin dropped below –1g, the simulated passenger came off the floor and impacted the 4-foot ceiling at approximately 2 seconds into the time history, see the time history of h. The relative velocity at impact was approximately 20 fps, see $\dot{h}$. However, after the acceleration reversed, the simulated passenger fell back down to the floor and impacted with an even greater velocity than before.

A matrix of gust lengths and gust amplitudes were run through the simulation program to produce time histories. A second program then extracted the maximum values of the accelerations and impact velocities. These data were then transformed into contour plots such as those shown in figure 5 for the normal acceleration at the c.g. As can be seen in the figure, the maximum accelerations are a function of both the gust length and the gust amplitude. For example, at a gust amplitude of –40 fps, the acceleration varies from 1.5 g's at a gust length of about 200-300 ft to only 0.5 g's at a gust length of about 2200 ft. However, at very short gust lengths the accelerations drop off again because of the unsteady lift effects used in the simulation.

The contour plots for the normal acceleration at the aft cabin location, figure 6, are practically identical to those at the c.g. at gust lengths greater than 1000 ft. However, at the shorter wavelengths, the aft cabin accelerations are significantly higher. Part of this increase is due to the pitching motion of the simulated airplane, but a significant part is due to the excitation of the structural mode of the tail. The combined effect of the pitching and structural mode is enough to offset most of the reduction due to the unsteady lift effects.

The contour plots of the equivalent fall heights are presented in figure 7. The maximum contours occur for gust lengths less than 500 ft. However, they drop off sharply for the smallest gust lengths despite the fact that the aft cabin accelerations were very high at the same gust lengths, figure 6. The reason for this, of course, is that for the shorter gust lengths the accelerations reversed so quickly that the resulting velocities and displacements were relatively small. In fact, for the shorter gusts the simulated passengers did not impact the ceiling at all, but only came off the floor a small distance before impacting with floor again.

Data from Accidents

Analysis equations:

The first step in the calculations was to calculate the change (delta) in the vertical acceleration and pitch attitude from the initial, undisturbed flight values, n_{ic} :and θ_{ic} :

$$\Delta n_{cg} = n - n_{ic} \quad \text{and} \quad \Delta\theta = \theta - \theta_{ic} \tag{30}$$

Next, the dynamic pressure was calculated from the true airspeed:

$$\bar{q} = \frac{1}{2}\rho(V)^2 \tag{31}$$

where ρ and V were derived from the pressure altitude and indicated airspeed assuming a standard atmosphere and zero position error corrections. The third step was to calculate the change in angle of attack from the change in vertical acceleration ignoring the effect of the elevator and other second-order parameters on the acceleration:

$$\Delta\alpha = \left(\frac{W}{\bar{q}S_w C_{L,\alpha}}\right)\Delta n_{cg} \tag{32}$$

The weight of the airplane was estimated from the accident records of the fuel and passenger load. The wing area, S_w, was determined from publicly available information on the aircraft type. The lift curve slope, $C_{L,\alpha}$, was estimated using aerodynamic data charts[4] and publicly available information on the wing and tail for each accident airplane.

The next step was to calculate the change in flight path angle from the vertical acceleration and true airspeed:

$$\Delta\gamma = \frac{g}{V}\int \Delta n_{cg}\, dt \tag{33}$$

It should be mentioned that the vertical acceleration, Δn_{cg}, in equations (32) and (33) included a small correction determined separately to make the second integral of Δn_{cg} more consistent with the changes in measured pressure altitude.

The final step was to calculate the change in the vertical gust velocity from the previously calculated parameters:

$$\Delta w_g = V(\Delta\alpha - \Delta\theta + \Delta\gamma) \tag{34}$$

Equation (34) is the NASA aircraft turbulence measurement equation[5] with the acceleration-derived angle of attack substituted for the vane-measured angle of attack.

Recovered gust velocities:

The recovered gust velocities for three different accidents are presented in figures 8 to 10. Each accident is different, but there are some common features. The gust amplitudes are very larger—up to 100 fps, and they attain their maximum values in a few seconds. Another interesting characteristic is that the largest magnitude accelerations are in the negative direction and they occur when the initial upward gusts reverse direction. The fact that all 3 accidents had their largest magnitude accelerations in the negative direction may be because the NTSB data collection process would naturally eliminate positive accelerations. That is, large positive accelerations will not generally throw passengers around the cabin so that these incidents do not result in accidents and would be omitted from the available data base. However, the correlation between gust reversal and the peak accelerations may indicate that there may be a control input phasing problem between the airplane and the gust that contributes to the accidents. This speculation is supported by accident #2, figure 9. From about 10 seconds to 15 seconds there is a strong oscillatory acceleration response that is not correlated with the gust velocity. This oscillatory response was produced by control inputs to the elevator. However, it is impossible to tell from the recordings whether the control inputs were produced by the autopilot or the pilot. There is a strong tendency to overcontrol the pitch attitude in severe gust encounters[6,7,8]. The autopilot usually has a relatively small effect[9]. In any case, the present sample of only 3 accidents is too small to generalize to the larger world.

Comparison of Simulation to Accidents

Although the regular gust shape used in the simulation was not the same as the irregular gust shape encounter in the real accidents, a comparison was attempted. That is, the time intervals in the accident data where the gust gradients and amplitudes were the greatest were analyzed. The gust amplitudes were non-dimensionalized by dividing by gT_{θ_2} or $mg/\rho V S_w C_{L,\alpha}$. This factor compensates for different air speeds V, wing loadings $\frac{W}{S_w}$, altitudes (through ρ), and aerodynamic characteristics $C_{L,\alpha}$. Likewise the gust length was normalized by dividing by the true airspeed to account for differences in the effective gust length due to different airspeeds. The results are presented in figure 11 for the cg acceleration. The accident data symbols are plotted according to the estimated maximum gust amplitudes

and gust lengths. Next to each symbol is a numerical value in parenthesis indicating the maximum recorded acceleration. By comparing the maximum recorded acceleration to the nearest simulated acceleration contour, a measure of the agreement between the two data can be made. It is apparent that the agreement is relatively poor for accident #1 and #2. In fact, the accelerations for those two accidents are over twice that predicted by the simulation. In other words, it appears that the accident accelerations were much larger than they would have been if the airplanes had responded to the given gusts in the same manner as the simulated airplanes. A more detailed analysis of the accidents indicated that the elevator control motions and pitching response were larger than those of the simulation. It was impossible to determine the reason for the larger control motions and pitching response from the limited number of parameters recorded on the flight recorders. That is, it could not be determined whether the autopilot or the pilot was making the control inputs. Only the data for accident #3 (good agreement with simulation) indicated the status of the autopilot showing that it was disengaged after the (positive) peak in the acceleration.

Concluding Remarks

A simple mathematical model for studying the longitudinal effects of gusts has been described. The model includes the effects of fuselage flexibility and the motion of an unrestrained mass (simulated passenger) in the aft passenger cabin. The model has been used to calculate the response to different gust shapes and amplitudes and flight conditions. However, only calculations for a mountain rotor gust profile are presented because of the similarity of the results for different wave shapes. Gust length was shown to be nearly as important as gust amplitude in predicting airplane response. The simulated passenger in the aft passenger cabin had the most severe collisions with the cabin interior for gust lengths of approximately 300-400 ft. However, aeroelastic effects on simulated passenger collisions with the cabin interior were minimal.

The model predictions have been compared to data from three airline turbulent accidents. The accelerations during the actual accidents were sometimes twice as large as the model predictions. This large difference may be due to the transients during the autopilot disconnect sequence or pilot control inputs. However, the accident data does not contain enough parameters to draw any firm conclusions.

References

1. Anon: In-Flight Safety of Passengers and Flight Attendants Aboard Air Carrier Aircraft; NTSB-AAS-73-1, March, 1973.
2. Jones, Robert T.: The Unsteady Lift of a Finite Wing. NACA TN 682, 1939.
3. Phillips, William H., and Kraft, Christopher C.: Theoretical Study of Some Methods for Increasing the Smoothness of Flight through Rough Air. NACA Technical Note 2416, July 1951.
4. Etkin, Bernard: Dynamics of Flight-Stability and Control. John Wiley and Sons, 1959.
5. Houbolt, John C.; Steiner, Roy; and Pratt, Kermit G.: Dynamic Response of Airplanes to Atmospheric Turbulence Including Flight Data on Input Response. NASA TR R-199, 1964.
6. Anon. Civil Aeronautics Board: Aircraft Accident Report SA-372; Northwest Airlines, Inc. Boeing 720B, near Miami Florida, February 12, 1963; Report Released June 4, 1965.
7. Andrews, William H.; Butchart, Stanley P., Sisk, Thomas R.; and Hughes, Donald L.: Flight Tests Related to Jet-Transport Upset and Turbulent-Air Penetration, NASA SP-83, May, 1965.
8. Bray, Richard S., and Larsen, William E.: Simulation Investigation of the Problem of Flying Swept-Wing Transport Aircraft in Heavy Turbulence; NASA SP-83, May, 1965.
9. Goldberg, Joseph H.: Gust Response of Commercial Jet Aircraft Including Effects of Autopilot Operations. NASA CR-165919, June 1982

Table I. Simulated Airplane Characteristics

Characteristic	**Value**
Weight, W	140,000 lb
Wing area, S_w	1994 ft^2
Zero lift drag coefficient of tail, $C_{Do,t}$	.01
Tail lift curve slope, $C_{L\alpha,t}$	1.19/rad
Wing downwash on tail, $\frac{\partial \varepsilon}{\partial \alpha}$	.55
Pitch moment of inertia, I_y	525,000 slug-ft^2
Efficiency factor of tail, k_t	.1058
Elevator effectiveness, $k_{\delta e}$	0.5
x location of wing aerodynamic center, x_w	-0.59 ft
z location of wing aerodynamic center, z_w	0.0 ft
x location of tail aerodynamic center, x_t	-76.6 ft
z location of tail aerodynamic center, z_t	0.0 ft
x location of thrust, x_T	0.0 ft
z location of thrust, z_T	0.0 ft
pitch gain in automatic control system, k_θ	2.0 rad/rad
pitch rate gain in automatic control system, k_q	0.3 rad/(rad/sec)
altitude gain in automatic control system, k_h	.0001 rad/ft
flexible tail spring constant, k	91,000lb/ft
flexible tail effective mass, m_e	257 slugs
Thrust	16074 lb
trim angle of attack, α_{trim}	0.67 degrees
trim elevator angle, $\delta_{e,trim}$	-0.89 degrees
trim flexible tail deflection, y_{trim}	0.0118 ft
flexible tail natural frequency, f	3 Hz
flexible tail stiffness factor, R	.02

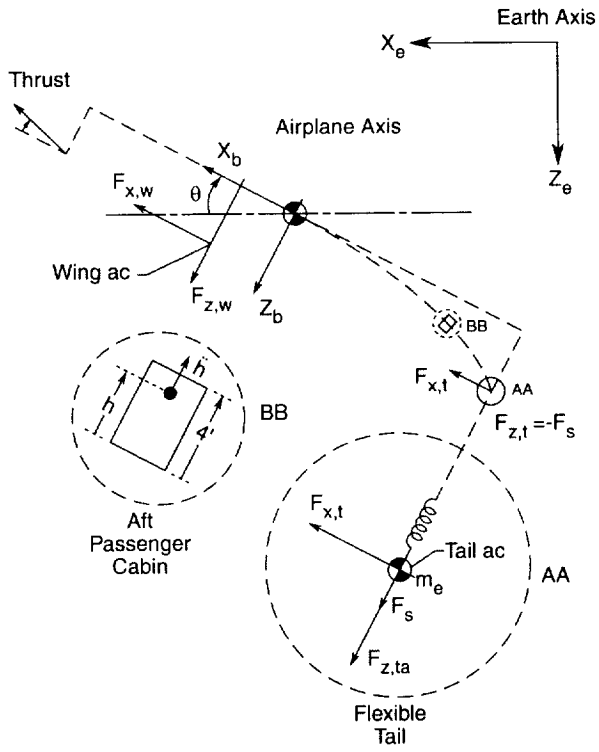

Figure 1. Schematic of simulated airplane math model showing the main components: wing, horizontal tail, elastic fuselage, and aft passenger cabin with an unrestrained mass.

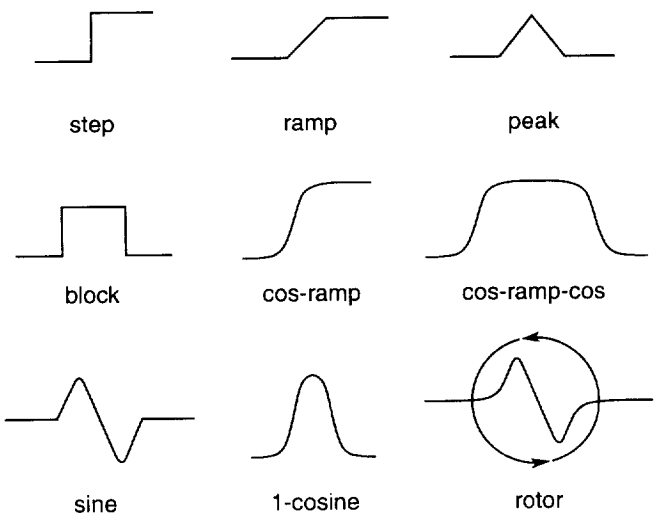

Figure 2. Sketches of some of the different gust wave shapes that were studied.

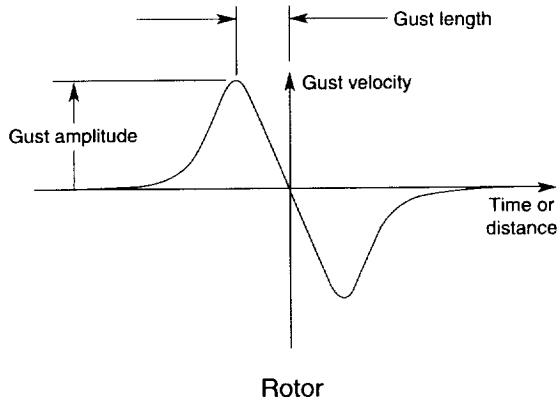

Figure 3. Sketch of the "mountain rotor" wave shape used in the simulation results presented herein.

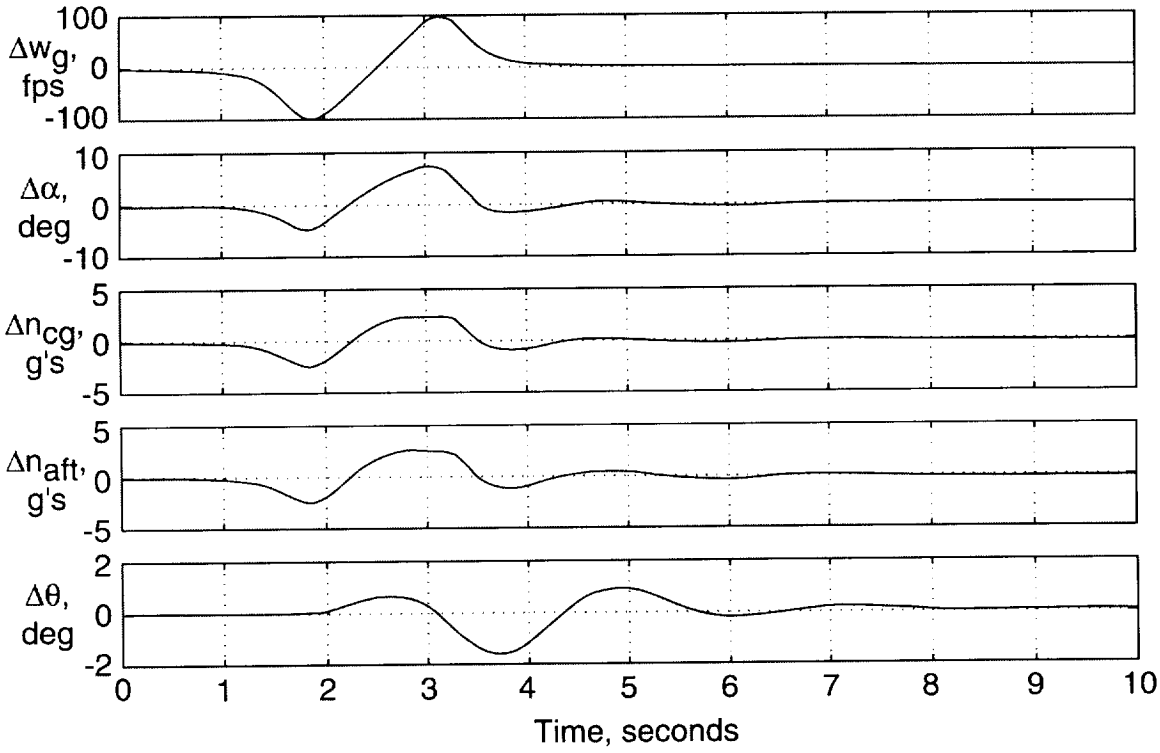

a) First five parameters

Figure 4. Time history of response to a –100 fps mountain rotor gust with a gust wavelength of 500 ft.

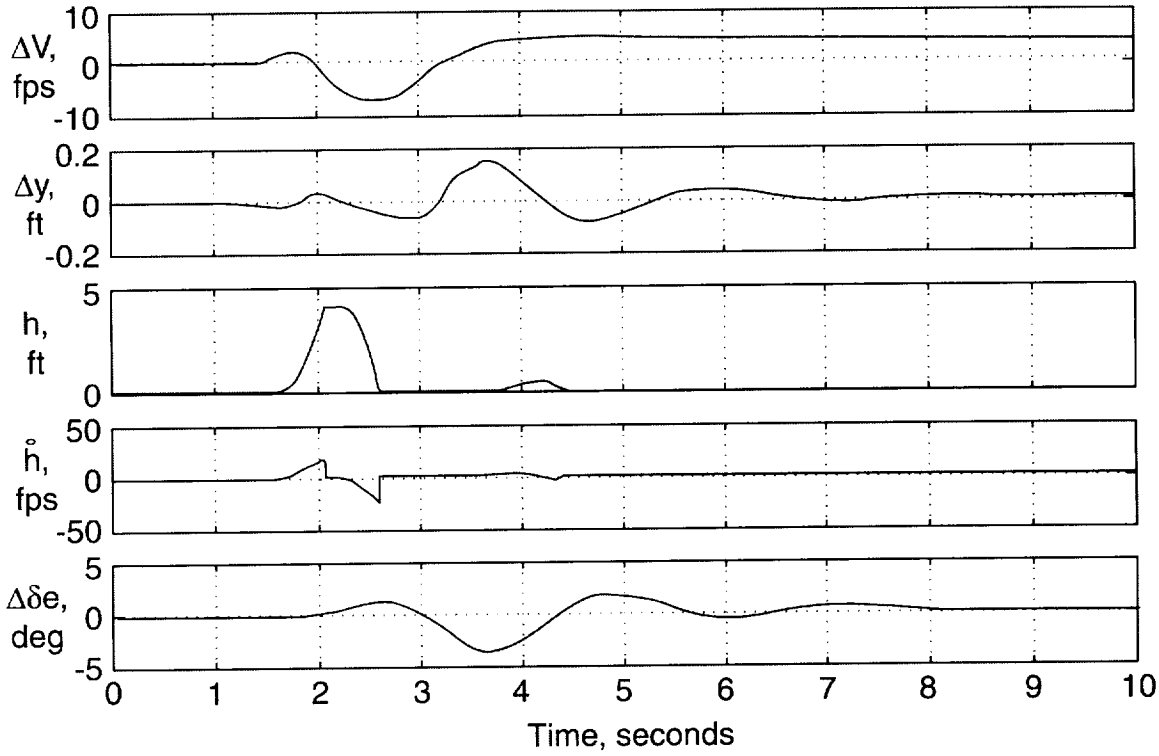

b) Second five parameters

Figure 4. Time history of responses to –100 fps mountain rotor with a gust length of 500 ft.

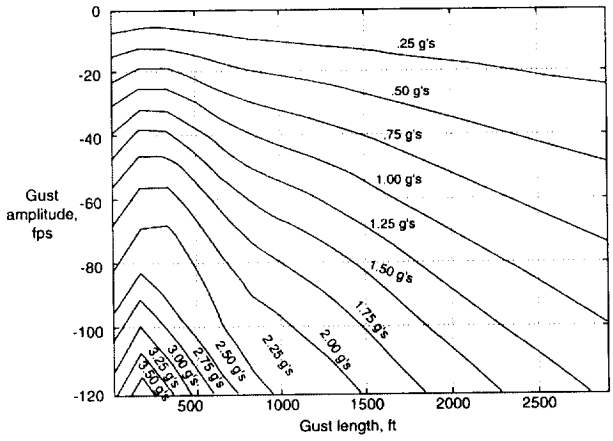

Figure 5. Contours of constant accelerations calculated at the center of gravity for mountain rotors with different gust lengths and gust amplitudes.

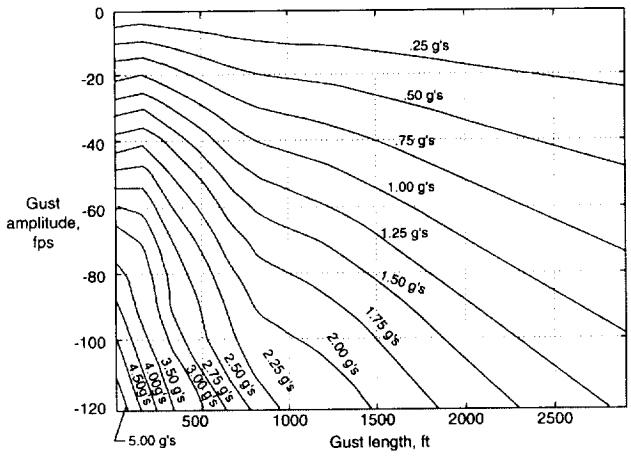

Figure 6. Contours of constant accelerations calculated at the aft passenger cabin for mountain rotors with different gust lengths and gust amplitudes.

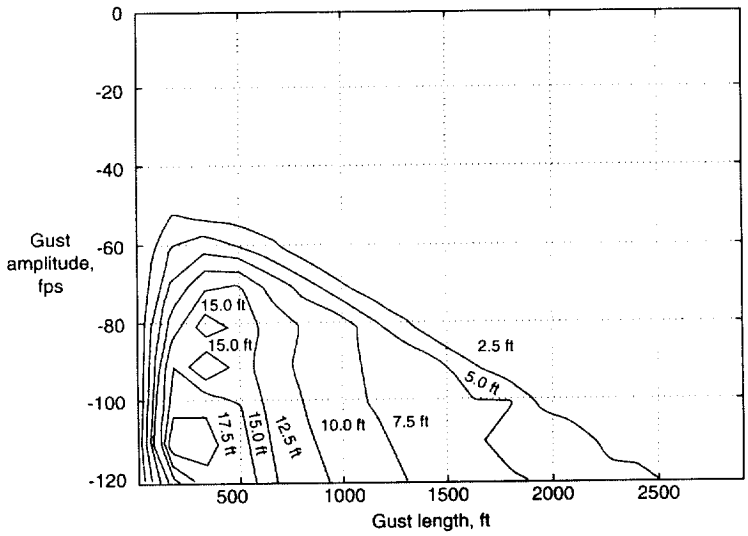

Figure 7. Contours equivalent fall heights calculated at the aft passenger cabin for mountain rotors with different gust lengths and gust amplitudes.

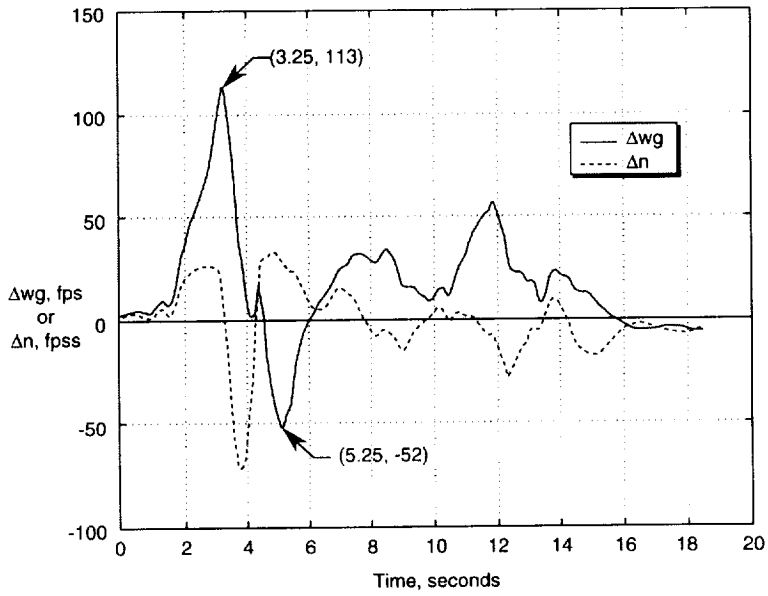

Figure 8. Accident #1, B737-200, August, 1997.

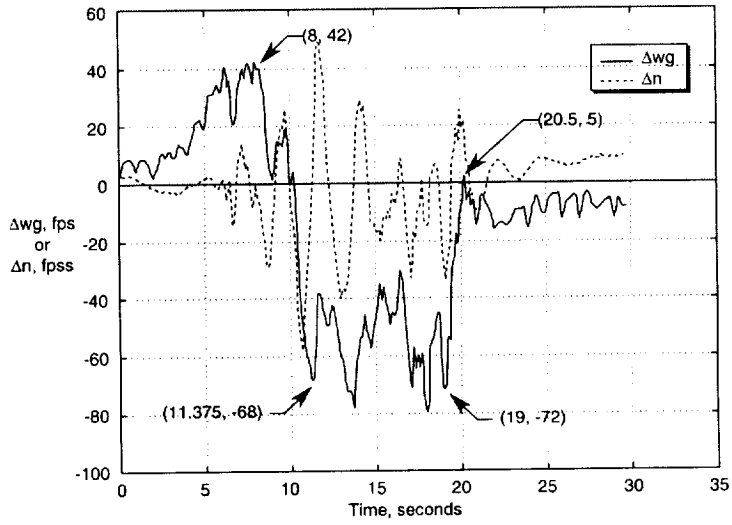

Figure 9. Accident #2, DC-9-51, January 1997.

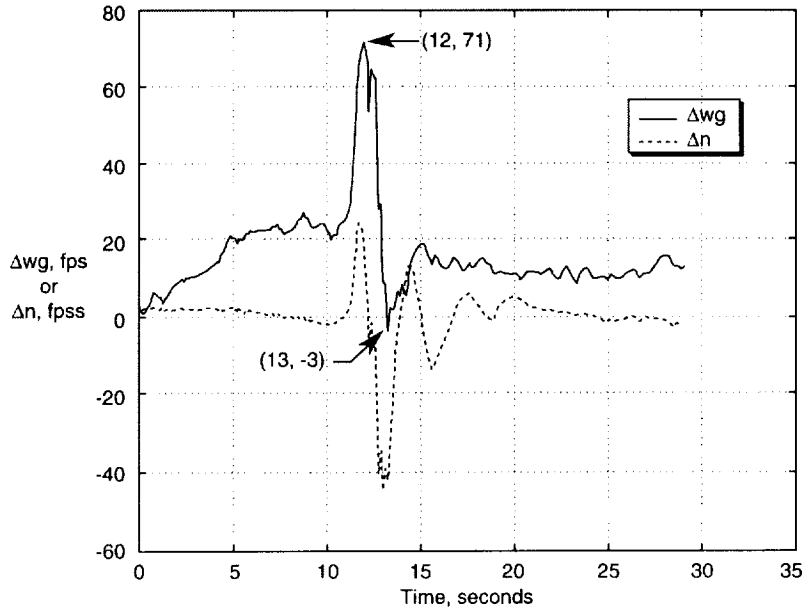

Figure 10. Accident #3, DC-9-82, October, 1997.

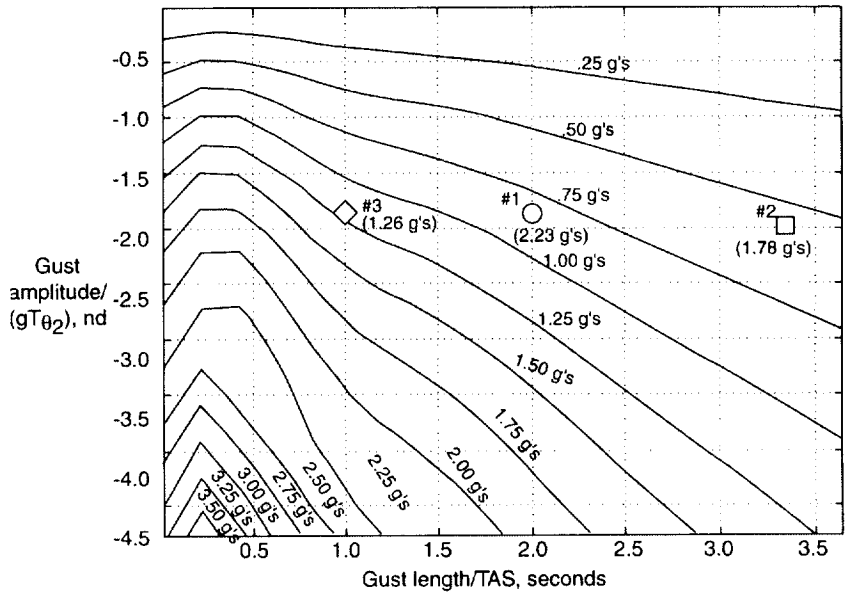

Figure 11. Comparison of simulation predictions with accident data.